© 2022. Published by The Company of Biologists Ltd | Development (2022) 149, dev200256. doi:10.1242/dev.200256

RESEARCH ARTICLE

Quantitative live imaging of floral organ initiation and floral meristem termination in *Aquilegia*

Ya Min*,‡,§, Stephanie J. Conway*,§ and Elena M. Kramer‡

ABSTRACT

In-depth investigation of any developmental process in plants requires knowledge of both the underpinning molecular networks and how they directly determine patterns of cell division and expansion over time. Floral meristems (FMs) produce floral organs, after which they undergo floral meristem termination (FMT); precise control of organ initiation and FMT is crucial to the reproductive success of any flowering plant. Using live confocal imaging, we characterized developmental dynamics during floral organ primordia initiation and FMT in *Aquilegia coerulea* (Ranunculaceae). Our results uncover distinct patterns of primordium initiation between stamens and staminodes compared with carpels, and provide insight into the process of FMT, which is discernable based on cell division dynamics that precede carpel initiation. To our knowledge, this is the first quantitative live imaging of meristem development in a system with numerous whorls of floral organs, as well as an apocarpous gynoecium. This study provides crucial information for our understanding of how the spatial-temporal regulation of floral meristem behavior is achieved in both evolutionary and developmental contexts.

This article has an associated 'The people behind the papers' interview.

KEY WORDS: *Aquilegia*, Floral meristem, Live imaging, Primordia initiation

INTRODUCTION

The spatial-temporal regulation of cell proliferation and expansion is a fundamental aspect of development in all multicellular organisms. It is particularly crucial in plants because programmed cell death and cell migration play no role in most developmental processes, whereas morphogenesis and organogenesis occur throughout the entire lifespan of a plant (Steeves and Sussex, 1989). Furthermore, growth in plants is driven by the interplay of cell division and cell expansion; while cell expansion is essential to growth, cell division often also plays a key part, particularly in early stages. The foundation of continuous growth in a plant is the presence of meristems, which are groups of cells that possess stem cell properties and are typically located at the tips of all growing axes. Meristem activities must be well regulated to maintain a pool of pluripotent cells while also giving rise to differentiating cells. Based on the types of tissues and organs produced, meristems can be categorized into several types. For example, vegetative meristems produce vegetative organs such as leaves; root apical meristems are responsible for the growth of roots; and in flowering plants there are inflorescence meristems, which give rise to reproductive branches and floral meristems (FMs), which produce floral organs in spirals or whorls (i.e. concentric rings). Meristems that produce leaves and roots are indeterminate by nature, meaning that they are active throughout the lifespan of a plant and can make new organs and tissues continuously. The properties of the inflorescence meristems are more variable, and whether they grow indeterminately or determinately (i.e. are only active for a certain period of time) differs across plant lineages (Kirchoff and Claßen-Bockhoff, 2013; Bartlett and Thompson, 2014). FMs, however, are always determinant because every FM is responsible for the production of one flower, and every flower terminates after the production of a relatively finite number of organs, typically culminating in carpels. These consistently determinate meristems are particularly interesting to study in terms of the spatial-temporal regulation of cell behaviors. On the one hand, just like other meristems, FMs need to maintain homeostasis of their stem cell pools to ensure the successive production of organs. On the other hand, this proliferation must be terminated at a specific time point during floral organ initiation, a process called floral meristem termination (FMT). FMT results in the loss of pluripotency of all the cells that remain in the FM, which will then be incorporated into production of the innermost organs of the flower.

A key component of investigating regulation of FM proliferation and FMT from a developmental perspective is obtaining a detailed understanding of cell division and expansion dynamics, and the eventual integration of gene expression data and cellular geometric data, both temporally and spatially (Refahi et al., 2021). Most previous work has relied on histology, scanning electron microscopy, *in situ* hybridization or immunolocalization, all of which require fixation and, in most cases, sectioning of the tissues, rendering the dynamics static (Sappl and Heisler, 2013; Prunet and Duncan, 2020). Recent advancements in live-imaging techniques have allowed researchers to analyze how gene activities regulate the spatial-temporal dynamic of cellular behaviors quantitatively, at unprecedented resolutions and in real time (Sappl and Heisler, 2013; Prunet and Duncan, 2020). Implementation of quantitative live imaging has provided answers to many long-standing questions in plant development, such as the timing of the establishment of adaxial/abaxial polarities during primordium initiation (Zhao and Traas, 2021), the functions of the gene *SUPERMAN* in regulating organ boundaries and FMT (Prunet et al., 2017), and the mechanisms generating the giant cells in the *Arabidopsis thaliana* sepals (Roeder et al., 2010). Therefore, to gain an in-depth understanding of the dynamics of meristem function, we need both

Department of Organismic and Evolutionary Biology, Harvard University, 16 Divinity Avenue, Cambridge, MA 02138, USA.
*Present address: Department of Ecology and Evolutionary Biology, University of Connecticut, Storrs, CT 06269, USA. §These authors contributed equally to this study.

‡Authors for correspondence (ya.min@uconn.edu, ekramer@oeb.harvard.edu)

Y.M., 0000-0002-7526-4516; S.J.C., 0000-0001-5058-6669; E.M.K., 0000-0002-5757-1088

Handling Editor: Ykä Helariutta
Received 9 October 2021; Accepted 31 December 2021

Development (2022) 149, dev200256. doi:10.1242/dev.200256

knowledge of different molecular regulatory networks and an understanding of how such networks directly control the precise actions of cell division and expansion over time, ideally in as many plant taxa as possible. So far, quantitative live imaging of meristems has only been developed for and applied to a small number of model species: the vegetative meristems of tomato, moss and *A. thaliana* (Reddy and Roy-Chowdhury, 2009; Harrison et al., 2009; Hamant et al., 2019); the inflorescence meristems of *Gerbera hybrida*, *Brachypodium distachyon* and *A. thaliana* (Heisler and Ohno, 2014; O'Connor, 2018; Zhang et al., 2021); the root meristems of *A. thaliana* (Rahni and Birnbaum, 2019); and the early FMs of *Cardamine hirsuta* and *A. thaliana* (Prunet et al., 2016; Monniaux et al., 2018).

In this study, we have applied a recently developed live confocal microscope imaging technique to produce the first quantitative characterization of the cellular dynamics in the FMs of *Aquilegia coerulea*, with a particular focus on FMT. *Aquilegia coerulea* is a member of the buttercup family (Ranunculaceae) and is a model system for evolutionary developmental studies with a well-annotated genome and a number of functional tools (Kramer, 2009; Filiault et al., 2018). We chose to focus on the developmental window of FMT because of its crucial role in flower development, but also because the cell dynamic changes during FMT have not yet been described quantitatively in any model systems. In addition, the FMs of *A. coerulea* have several significant differences compared with the FMs of *A. thaliana*, one being that they are maintained for a longer period before FMT to allow for the production of 15-17 whorls of floral organs compared with the four whorls of organs in *A. thaliana*. Moreover, FMT is very different between these two systems from a morphological perspective. After FMT, the carpel primordia of *A. thaliana* arise as a single syncarpous gynoecium (Hill and Lord, 1989), incorporating all of the cells that remained in the apex of the FM. In contrast, carpels of *A. coerulea* comprise an apocarpous gynoecium, formed by five distinct and unfused primordia, such that the apex of the FM is not spontaneously consumed by their emergence (Tucker and Hodges, 2005). Currently, we have no information regarding how different patterns of carpel primordia initiation influence FMT in flowering plants.

By imaging the same *A. coerulea* FMs in tissue culture at repeated time intervals and using the software MorphoGraphX (Barbier de Reuille et al., 2015), we conducted lineage tracing of cells, and quantified the rate and distribution of cell division, as well as the degree and direction of cell expansion, over multiple developmental stages. Our results have revealed how the dynamics between cell proliferation and expansion change as the FM transitions from production of stamens to staminodes to carpels, allowing a detailed description of the initial developmental stages of floral organ primordia. To our knowledge, this study is the first quantitative live imaging of meristem development in a system with numerous whorls of floral organs and an apocarpous gynoecium, and is the first cellular characterization of FMT. Our results will lay the foundation for investigating gene expressions in the *A. coerulea* FMs in real-time, providing crucial information for our understanding of how the spatial-temporal regulation of meristem behavior is achieved in both evolutionary and developmental contexts.

RESULTS

The developmental window covered in the study

The *A. coerulea* flower is composed of five organ types, which, arranged from outermost to innermost, are the sepals, petals, stamens, staminodes and carpels (Fig. 1; Fig. S1). The five sepals are initiated in spiral phyllotaxy, whereas all other organs are produced synchronously in whorls of five (Fig. 1D). Each adjacent whorl initiates in alternating positions, either directly above the sepals or the petals, resulting in 10 orthostichies (i.e. vertical rows of organs) (Fig. 1C-E). Each flower consists of one whorl of sepals, one whorl of petals, an average of 10 to 12 whorls of stamens, two whorls of staminodes and one whorl of carpels. As we have focused on the later stages of FM development in the current study, the FMs we dissected for live imaging had typically initiated 8-10 whorls of stamens. For each stage, we designate the youngest primordial whorl as 1 and the previous whorl as 1+*n*; therefore, sd1 represents the inner whorl of staminodes that are produced after sd2, and st1 represents the last whorl of stamens initiated in the flower (Fig. 1E). In addition, we define 'newly emerging primordia (NEP)' as the youngest organ primordia of the floral bud, which just bulges out at the periphery of the meristem and can be distinguished morphologically; while the 'incipient primordia (ICP)' are the primordia that are initiating after the NEP but cannot yet be distinguished morphologically. Both NEP and ICP can be visualized by examining expression of the previously studied abaxial polarity gene *FILAMENTOUS FLOWER* (*AqFIL*) in *Aquilegia* (Fig. 1F; Meaders et al., 2020).

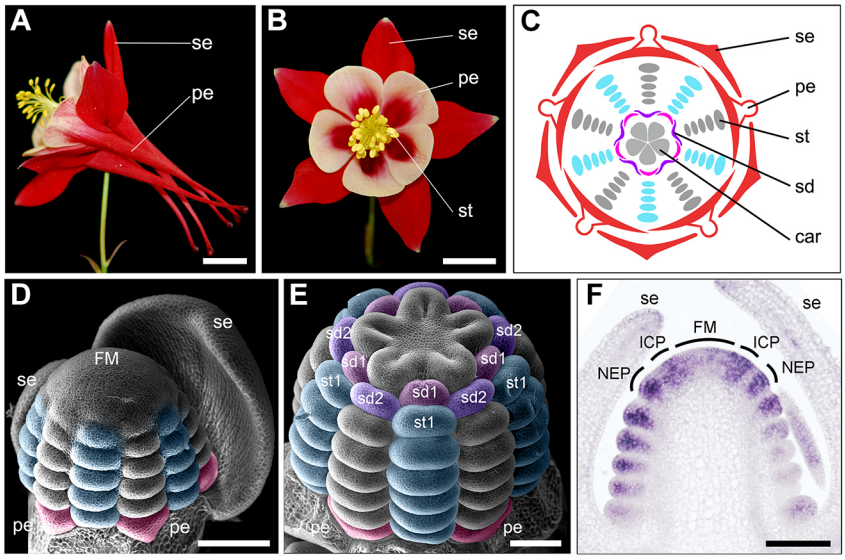

Fig. 1. Floral morphology of *A. coerulea* flowers. (A) Side view of a mature flower. (B) Front view of a mature flower. (C) Floral diagram of a typical *A. coerulea* flower. (D) A young FM in the process of producing stamens. (E) A young floral bud in the initial stage of carpel development. (F) *In situ* hybridization of abaxial identity gene *AqFIL* in a young *A. coerulea* FM. Expression pattern courtesy of C. Meaders (University of California, San Diego, USA). se, sepals; pe, petals; st, stamens; sd, staminodes; car, carpels; st1, the last whorl of stamens initiated in the flower; sd1, the center-most whorl of staminodes; sd2, the whorl of staminodes produced after st1 and before sd1; FM, floral meristem; ICP, incipient primordia; NEP, newly initiated primordia. Scale bars: 1 cm in A,B; 100 µm in D-F.

Development (2022) 149, dev200256. doi:10.1242/dev.200256

We used a 48 h imaging interval because we have observed that a new whorl of stamen or staminode primordia became visible roughly every 48 h in our experimental conditions, and almost all cells that underwent a cell division during this imaging interval divided only once. Based on this imaging interval, we defined six time points (TPs) in our study, resulting in five comparative developmental windows (Fig. 2; Fig. S2). The first four TPs are distinguished by the successive initiation of floral organ whorls: st1

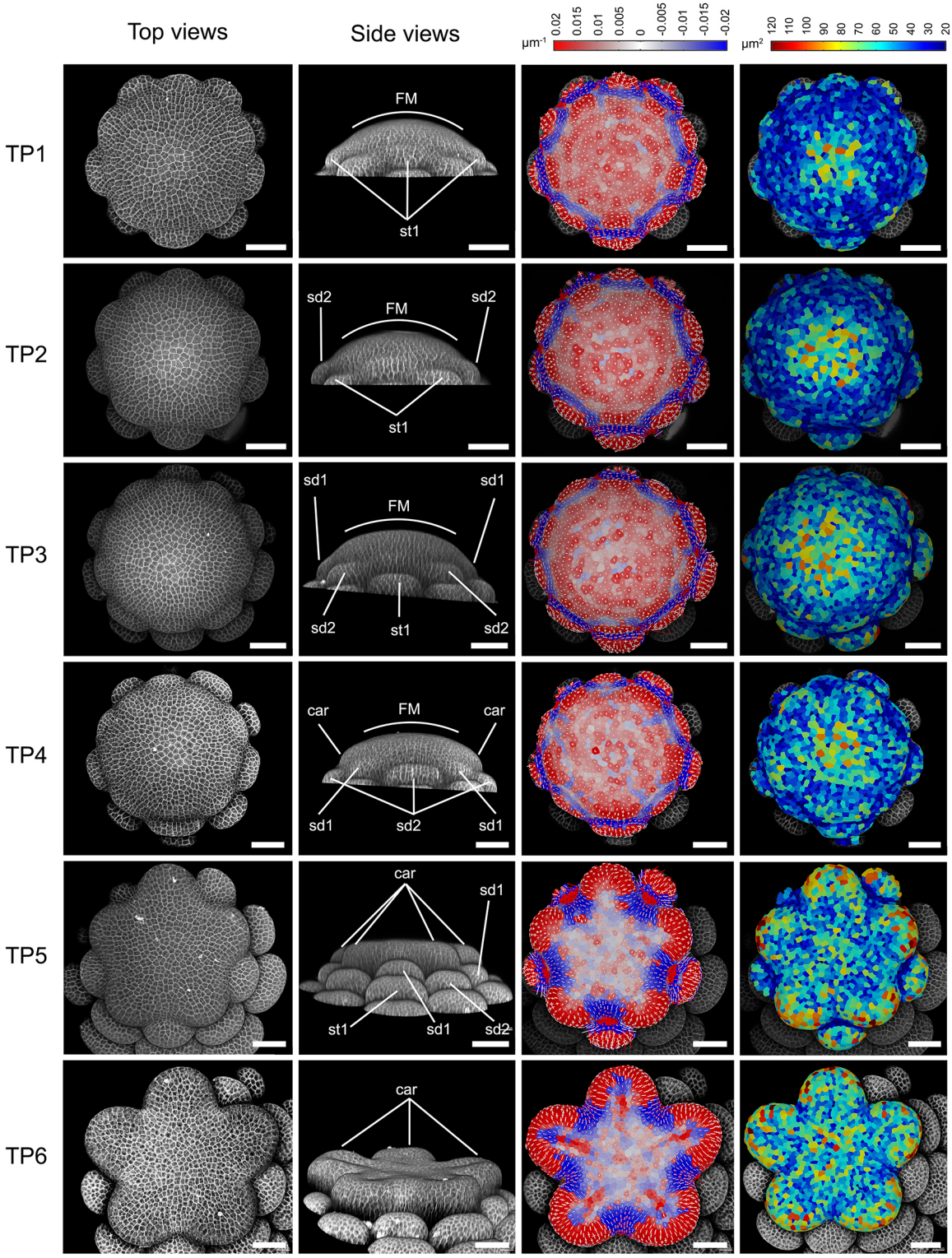

Fig. 2. Developmental windows covered in the current study. Columns from the left to the right are the top view, side view, top view with curvature heatmap and cell area heatmap of each time point 1-6 (TP1-6). All surface curvature heatmaps or cell area heatmaps used the same heatmap scale that is positioned above the respective column. car, carpel primordia; st1, the last whorl of stamens initiated in the flower; sd1, the center-most whorl of staminodes; sd2, the whorl of staminodes produced after st1 and before sd1. Scale bars: 50 μm.

Development (2022) 149, dev200256. doi:10.1242/dev.200256

during TP1; sd2 during TP2; sd1 during TP3; and carpels during TP4. At TP5, the five carpel primordia formed a completely flat, star-shaped apex. At TP6, the carpel primordia each form an elevated ridge at their distal periphery. The meristematic dome was maintained until TP4, at which point the initiation of the carpel primordia resulted in flattening of the apex (Fig. 2). The overall distribution of observed cell sizes was consistent with previous observations (Steeves and Sussex, 1989) that cells in the center of the apex are generally larger than the cells in the peripheral regions (Fig. 2).

Overall growth dynamics over the developmental windows

We used the imaging data to conduct lineage tracing of the epidermal cells of the floral apices to quantify their growth dynamics (Fig. 3). To determine whether there were any quantifiable differences in the patterns of growth between the TPs, we constructed growth alignment graphs by plotting the cell area expansion rates and the average number of cell divisions based on the locations of cells along the radial axis of each apex (Fig. 3, Fig. S3). For each apex, these radial transects were calculated from the center of the floral apex to the inner edges of the NEP whorl based on the curvature heatmap, dividing the transects into six equal bins (Fig. S3).

All developmental windows showed a general pattern that cell area expansion rates were lower at the center and higher at the periphery close to the NEP, but the overall expansion rates after TP4 (i.e. carpel primordia initiation; Fig. 3D-E′,F) were significantly lower than the earlier developmental windows (Table S1). The area expansion rates were relatively consistent across the entire meristem between TP2 and TP3 (Fig. 3B,B′,F), during which the sd1 primordia initiate. The cell area expansion rate displayed the largest difference between cells at the center and the periphery during the transition from TP4 to TP5 (Fig. 3D,D′,F), when the newly initiated carpel primordia were forming the flat star apex. Interestingly, the TP5 to TP6 (Fig. 3E,E′) window showed very similar cell area expansion patterns compared with TP4 to TP5 (Fig. 3D,D′), only differing in cells close to the periphery, in which the cell area expansion rates are significantly higher in TP4 to TP5 (Fig. 3F; Table S1).

Overall, rates of cell division were uniformly low in the center of the meristems across all time points (Fig. 3D-E′,F), although there was a significant increase between TP3 and TP,4 preceding initiation of the carpel primordia (Fig. 3C,C′; Table S1). Moving outward in the meristems, rates of cell division generally increased progressively, regardless of the stage (Fig. 3). The one distinct exception was in TP5-TP6, during which rates were dramatically low in the center but sharply increased in the third bin domain, a pattern that was statistically different from the other stages (Fig. 3F; Table S1).

Floral organ primordia initiation

Subsequently, we analyzed how the initial outgrowth of organ primordia was achieved. Using st1 primordium initiation as an example, at TP1 the physical bulging of the primordia became visible (Fig. 4A,D,G). To precisely describe the growth each primordium, we defined the lateral axis as the axis that is parallel to the circumference of the dome of the FM, and the radial axis as the axis that runs from the center of the meristem to the center of the primordium (Fig. 4A). At TP1, Fig. 4A shows 10 cells of this NEP that are outlined in blue, representing the majority of the cells that exhibited positive surface curvature (i.e. are physically bulging out) compared with their surrounding cells, while the 10 cells outlined in green mainly had negative surface curvature (Fig. 4D). This includes part of the boundary region that separates this NEP from the primordium in the whorl positioned below (Fig. 4D). At TP2, the cells of the green domain, which have become the abaxial surface of the primordium (Fig. 4E), were the only cells that exhibited high growth rates during this developmental window (Fig. 4H). Cell division occurred on both the abaxial and adaxial sides (Fig. 4H), suggesting that this higher growth rate was mainly associated with cell expansion, which was supported by the cell anisotropy map (Fig. 4J). Cells on the abaxial side exhibited strong anisotropy along the radial axis, whereas cells on the adaxial side almost exclusively showed cell expansion along the lateral axis (Fig. 4J). At TP3, cell division occurred on both adaxial and abaxial sides of the primordium, and almost all cells in the primordium were exhibiting relatively high growth rates (Fig. 4I). The direction of cell expansion for the abaxial cells was more isotropic at this point (Fig. 4K). If the width of a cell along a given axis is decreased during the interval, it indicates compression rather than expansion. Interestingly, the adaxial-most layer of the cells at TP3 experienced significant compression along the radial axis while continuing to expand along the lateral axis (Fig. 4K), indicating these cells were incorporated into the formation of the organ boundary.

This phenomenon, that the initial outgrowth of the primordium was mainly achieved by high growth rates of the abaxial cells, was also observed for the initiation of staminode and carpel primordia (Fig. 5). Before entering the rapid growth phase, the abaxial cells initially comprised only one or two layers and were fewer than 10 cells wide (e.g. sd1 in Fig. 5A and car in Fig. 5B). These cells were located at the abaxial-most position of the ICP, and many (if not most) of them had negative surface curvatures (e.g. sd1 in Fig. 5D and car in Fig. 5E). They then exhibited substantial directional cell expansion along the radial axis, coupled with cell divisions so that they quickly made up half of the primordium (e.g. sd1 in Fig. 5H,J and car in Fig. 5I,K). Subsequently, the cells on the adaxial side started to exhibit relatively strong growth, and the direction of expansion of most of the cells in the primordium became more isotropic (e.g. sd1 in Fig. 5K).

In addition, we observed that after the initial strong growth phase in the abaxial cells, the primordia of sd1 displayed a lower overall growth rate than other NEPs; e.g. sd1 in Fig. 5H versus sd2 in Fig. 5I. This observation was confirmed by quantifying the number of cells that exhibited growth rates above 1.8 in ICP and NEP of different developmental windows (Fig. 5L). During the developmental window TP2 to TP3, in which the sd1 was the ICP, these primordia had similar numbers of cells exhibiting high growth compared with ICP and NEP of other stages. However, once the floral buds enter the TP3 to TP4 window, in which the carpels were the ICP and sd1 was the NEP, the number of sd1 cells exhibiting high growth decreased significantly (Fig. 5L).

Of the cells that exhibited high growth rates in the ICP and NEP of different developmental windows, we asked what percentage experienced cell division during the interval. We did not observe any significant difference between primordia of different windows (Fig. 5M) and, on average, about 50% of the cells exhibited both high growth and experienced cell division. We also examined the orientations of the division planes among these cells, and found that although there was no significant difference between primordia of different stages and developmental windows, most of the cell divisions occurred parallel to the lateral axis (Fig. 5N).

Early carpel development

We then analyzed the initial development of the carpel primordia, with a particular focus on three diagnostic regions: the distal edge, the primordial boundary and the adaxial fold (Fig. 6A). From TP4 to TP6, the width of the distal edge increased both along the lateral axis

Development (2022) 149, dev200256. doi:10.1242/dev.200256

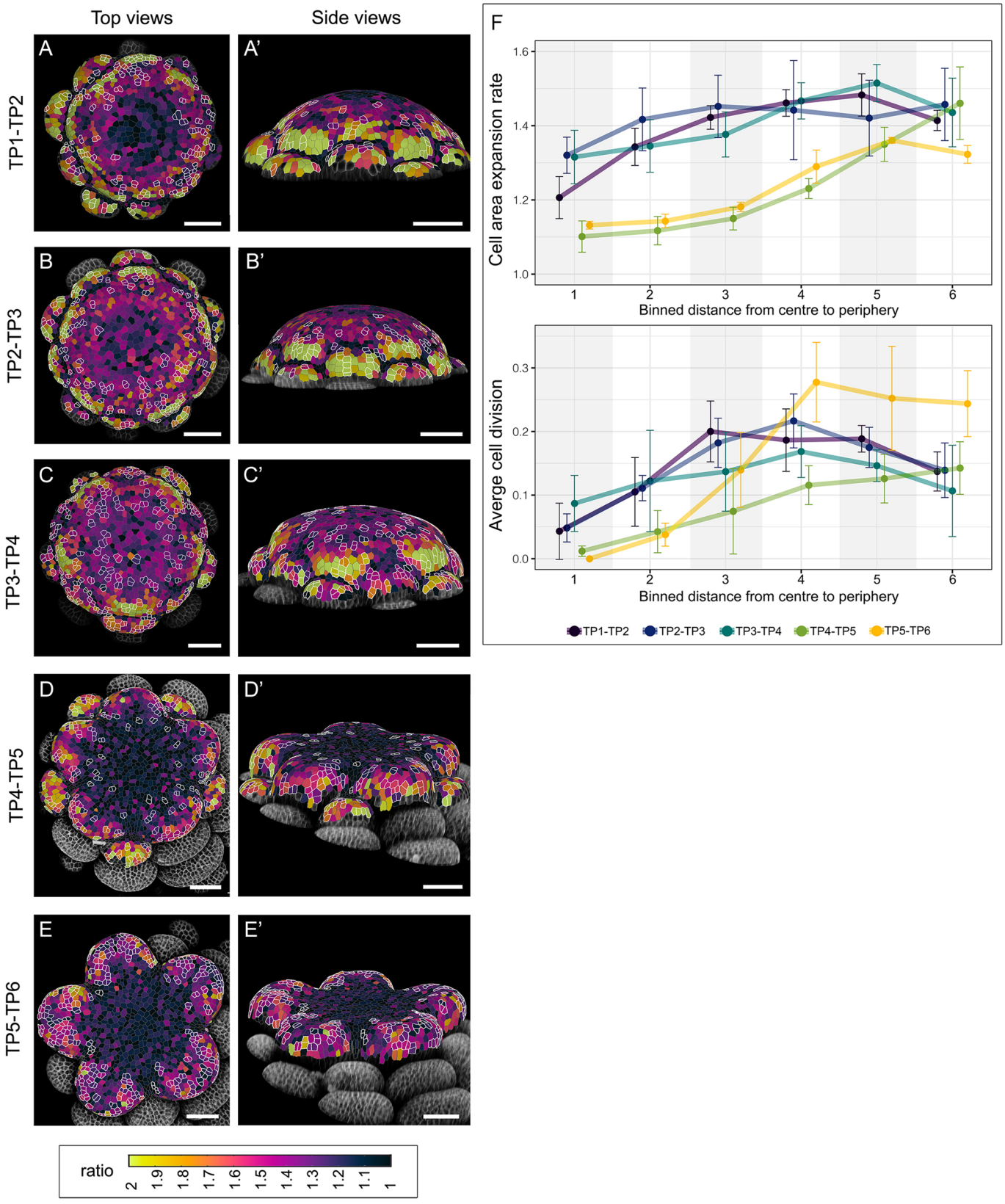

Fig. 3. Overview of growth dynamics in each developmental window. (A-E′) Heatmaps showing the area expansion rates of all cells between two successive time points (TPs). If a cell has divided during the imaging interval, the sum of the cell areas of the daughter cells is compared with the area of the mother cell. All cells that experienced cell division during the interval are outlined in white. All heatmaps used the same scale shown at the bottom. (F) Transects of cell growth from the center of the meristem to the most recently initiated primordia. These growth alignment graphs compare the cell area expansion rates (upper panel) and the average number of cell divisions (lower panel) between different developmental intervals. Data are mean±s.e.m. of three (TP5 and TP6) or four (TP1-TP4) biological replicates for each developmental interval. Scale bars: 50 µm.

Development (2022) 149, dev200256. doi:10.1242/dev.200256

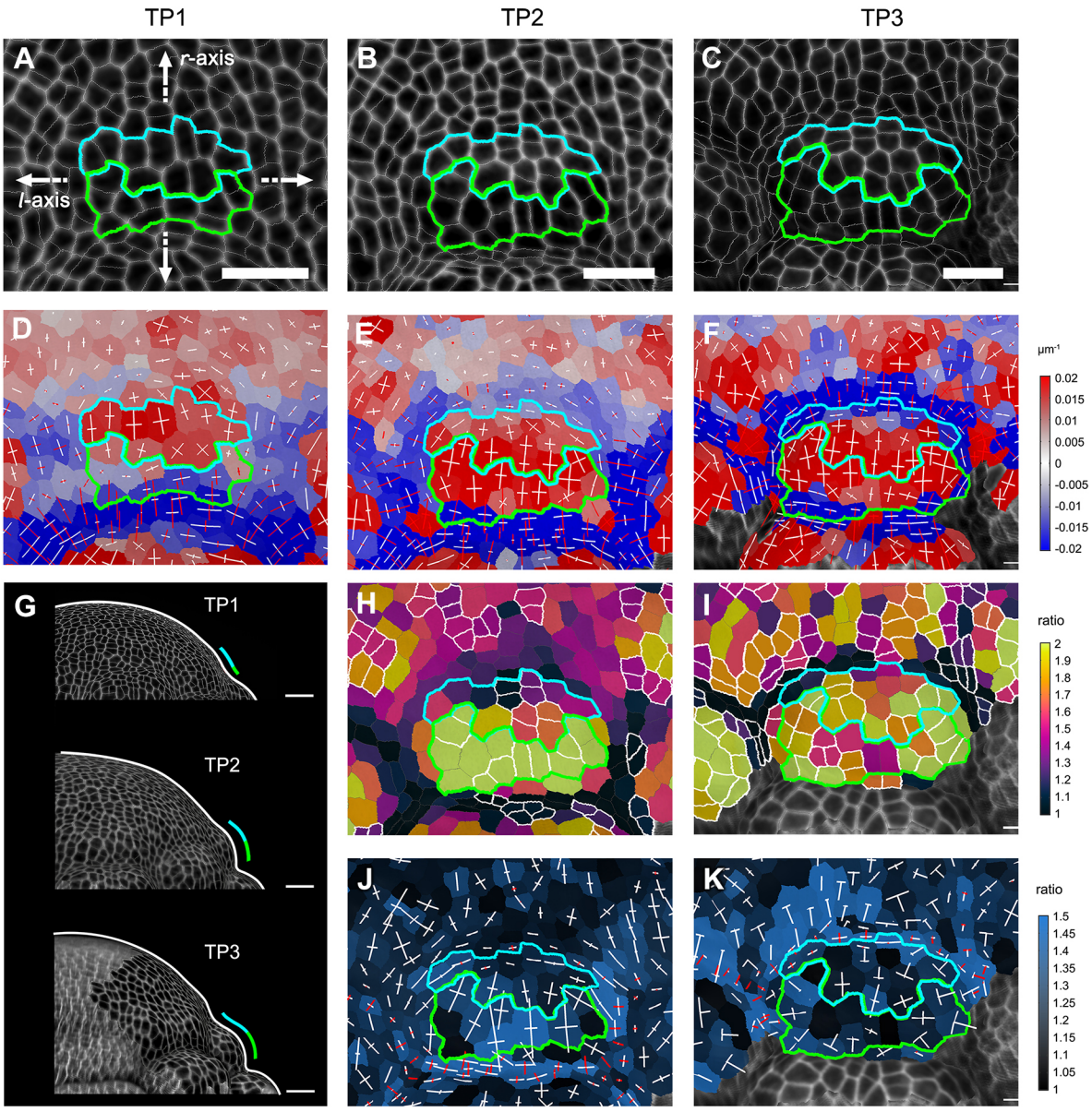

Fig. 4. Initiation of st1 primordia. (A-C) Front view of a st1 primordium at TP1 (A), TP2 (B) and TP3 (C). Cells outlined in green show the highest growth rates at TP1-TP2 (H), while cells outlined in blue show the highest curvature at TP1 (D). (D-F) Surface curvature heatmaps of A (D), B (E) and C (F). (G) Side views of the floral meristem (FM) at the equivalent TPs. The white line outlines the overall shape of the FMs, while the blue and green lines indicate the side view of the st1 primordium. (H,I) The cell area expansion heatmaps between TP1 and TP2, and TP2 and TP3, overlaid on B and C, respectively. Cells outlined in white are cells that experienced cell division during the interval. (J,K) Cell expansion anisotropy heatmaps between TP1 and TP2, and TP2 and TP3, overlaid on B and C, respectively. The color of a cell represents the value of the ratio between the changes in the longest axis and the shortest axis during the interval; lines inside the cell represent the degree and direction of cell expansion. White and red lines show the expansion (i.e. increase in length) or compression (i.e. decrease in length) of the cell shape along the indicated axis, respectively. *r*-axis, radial axis; *l*-axis, lateral axis. Scale bars: 20 μm in A-F,H-K (bar in A applies to D, bars in B and C apply to E,H,J and F,I,K, respectively); 50 μm in G.

and the radial axis, and the curvature of most cells increased (Fig. 6B-D). Over the same period, the primordial boundary became more folded towards the center of the apex (Fig. 6E-G). At TP4 and TP5, the regions that would become the adaxial folds transition from having positive surface curvature to having close to zero (i.e. flat) surface curvature (Fig. 6H,I). At TP6, invagination of the adaxial fold appeared to initiate at the base of the primordium and propagate outward, such that the proximal region was more deeply folded than the distal region at this stage (Fig. 6J).

Once the five carpel primordia were initiated, two processes happen simultaneously to achieve the flat star shape (Fig. 6). First, cells at the distal edges of the carpel primordia continued to display relatively high growth rates (Fig. 6C′), while cells at the center of the floral apex exhibited much lower overall growth rates (Fig. 3). This had the effect of elevating the carpel primordia to the same level as the center of the floral apex. However, unlike the early initiation of the carpel primordia, during which growth was mainly driven by the strong anisotropic expansion from the abaxial cells (Fig. 5I, K), the overall anisotropy of the cells on the carpel primordia distal edges was lower and less directional (Fig. 6C″). Meanwhile, numerous cells underwent cell division during this developmental window, suggesting that growth was strongly associated with cell division (Fig. 6C′). Second, cells at the primordial boundaries experienced strong compression along the lateral axis (Fig. 6F″),

Development (2022) 149, dev200256. doi:10.1242/dev.200256

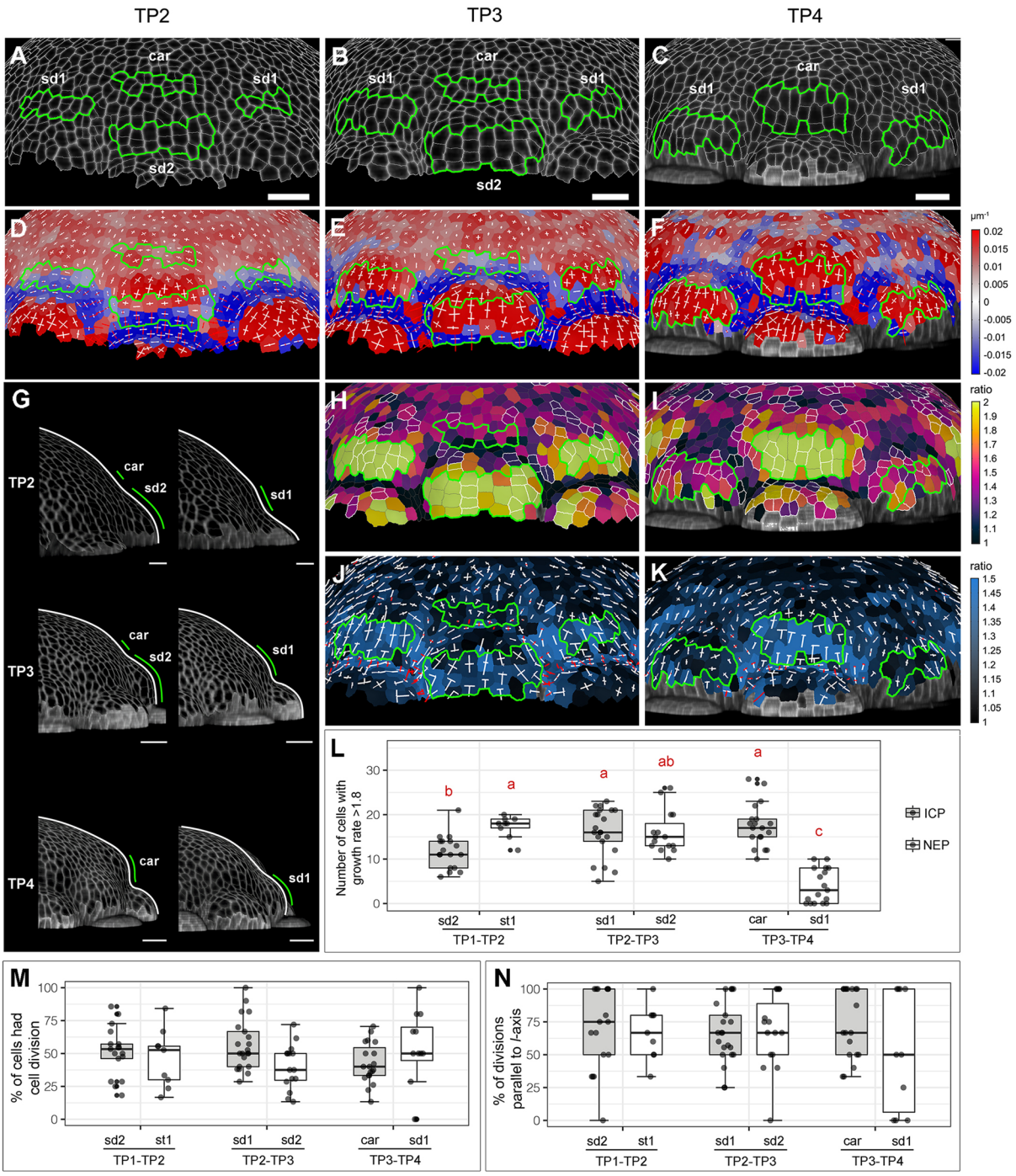

Fig. 5. Initiation of staminode and carpel primordia. (A-C,H,I) Front view of the sd1, sd2 and car primordia at TP2 (A), TP3 (B) and TP4 (C). The cells outlined in green are the abaxial cells of interest of the initiating primordia, as defined by high growth rates during TP2-TP3 (H) or TP3-TP4 (I). (D-F) Surface curvature heatmaps of A (D), B (E) and C (F). (G) Side views of the FM at different TPs. The white line outlines the overall morphology of the FMs and the green line indicates the position of the primordia of interest. (H,I) Cell area expansion heatmaps between TP2 and TP3, and TP3 and TP4, overlaid on B and C, respectively. Cells outlined in white resulted from cell division during the interval. (J,K) Cell expansion anisotropy heatmap between TP2 and TP3, and TP3 and TP4, overlaid on B and C, respectively. The color of a cell represents the value of the ratio between the changes in the longest axis and the shortest axis during the interval, and lines inside of the cell represent the degree and direction of cell expansion. White or red lines show the expansion (i.e. increase in length) or compression (i.e. decrease in length) of the cell shape along the indicated axis, respectively. (L) Comparisons of the number of cells with growth rates greater than 1.8 in primordia of different stages and developmental windows. Different letters above the boxplots represent significant differences between different primordia (P<0.05, using ANOVA followed by Tukey's pairwise multiple comparisons). (M) Comparisons of the percentages of cells that had growth rates greater than 1.8 and also experienced cell division during different time points. No significant difference was detected between different primordia using ANOVA. (N) Comparisons of the orientation of cell division among the cells that both had growth rates greater than 1.8 and experienced cell divisions. No significant difference was detected between different primordia using ANOVA. For L-M, each data point is a primordium; for each developmental window, at least three FMs were quantified. For each time period, the identity of the ICP changes and there is a NEP shift. For example, sd2 are the ICP at TP1-TP2 but become the NEP at TP2-TP3. In L-N, the boxplots show the median, quartiles, minimum and maximum values in each data group. Scale bars: 20 μm in A-F,H-K (bar in A applies to D, bars in B and C apply to E,H,J and F,I,K, respectively); 50 μm in G.

Development (2022) 149, dev200256. doi:10.1242/dev.200256

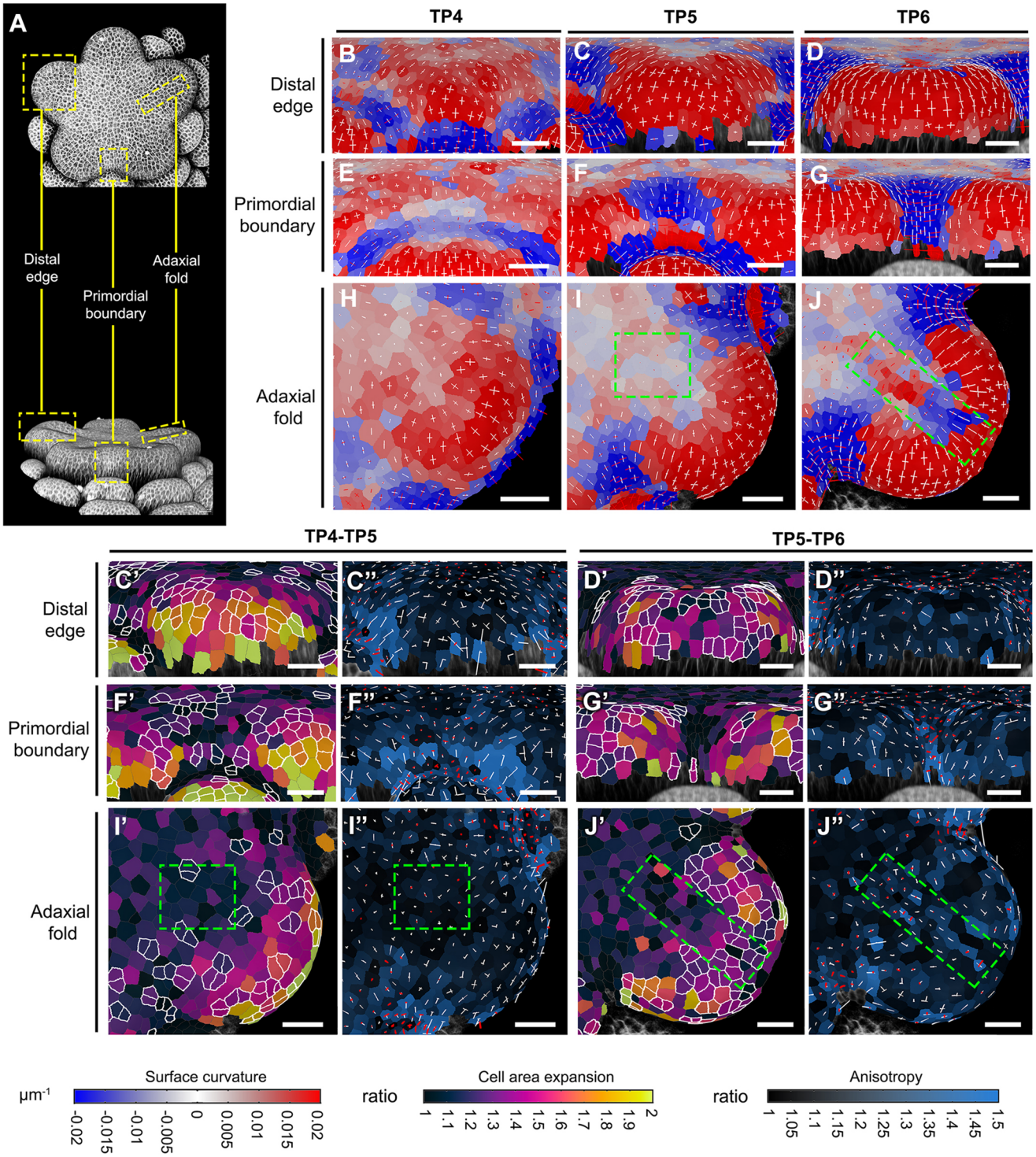

Fig. 6. Early carpel primordia development. (A) Top view and side view of an *A. coerulea* floral meristem (FM) at TP6 to indicate different regions of interest. (B-D) Side views of the surface curvature heatmaps of the distal edges of carpel primordia at TP4 (B), TP5 (C) and TP6 (D). (E-G) Side views of the surface curvature heatmaps of the primordial boundaries between carpels at TP4 (E), TP5 (F) and TP6 (G). (H-J) Front view of the surface curvature heatmaps of the adaxial folds of carpel primordia at TP4 (H), TP5 (I) and TP6 (J). (C′,C″) Heatmaps of cell area expansion (C′) and anisotropy (C″) of distal edges between TP4 and TP5 overlaid onto TP5. (D′,D″) Heatmaps of cell area expansion (D′) and anisotropy (D″) of distal edges between TP5 and TP6 overlaid onto TP6. (F′,F″) Heatmaps of cell area expansion (F′) and anisotropy (F″) of primordial boundaries between TP4 and TP5 overlaid onto TP5. (G′,G″) Heatmaps of cell area expansion (G′) and anisotropy (G″) of primordial boundaries between TP5 and TP6 overlaid onto TP6. (I′,I″) Heatmaps of cell area expansion (I′) and anisotropy (I″) of adaxial folds between TP4 and TP5 overlaid onto TP5. (J′,J″) Heatmaps of cell area expansion (J′) and anisotropy (J″) of adaxial folds between TP5 and TP6 overlaid onto TP6. Cells outlined in white in all cell area expansion heatmaps were cells that experienced cell divisions during the intervals. In all cell area expansion and anisotropy heatmaps, white or red lines show the expansion (i.e. increase in length) or compression (i.e. decrease in length) of the cell shape along the indicated axis, respectively. Green dashed boxes in I-J″ indicate the adaxial folds. All distal edge panels are the side view of the distal edge; all primordia boundary panels are the side views of the primordial boundary; all adaxial fold panels are the front view of the adaxial fold. Scale bars: 20 µm.

Development (2022) 149, dev200256. doi:10.1242/dev.200256

which helped to define the primordial boundary regions of the flat star shape. Interestingly, at this stage, although the floral apex was flat and the adaxial folds were not yet physically visible (Fig. 6I), minor compression of cells in the future location of the adaxial fold can already be observed (Fig. 6I″).

After formation of the flat star apex, the carpel primordia began to elevate along their distal ridges, which was mainly achieved by concentrated cell divisions on the ridges (Fig. 6D′,J′), while the anisotropic expansion rates of cells on the ridges remained low (Fig. 6D″). The growth alignment graphs in Fig. 3 also support this observation of concentrated cell divisions in the peripheral region relative to the earlier developmental windows (Fig. 3). Meanwhile, the cells at the primordial boundaries continued to experience strong compression along their lateral axis. We did not observe any further cell division in the primordial boundaries (Fig. 6G′,G″). In addition, the adaxial folds of the carpels have become morphologically visible (Fig. 6J), exclusively achieved by modifications in cell shape as no cell division occurred in the region (Fig. 6J′). Specifically, cells of the adaxial fold located closer to the center of the floral apex experienced strong compression, whereas those in the distal region of the adaxial fold exhibited strong anisotropic expansion along the radial axis (Fig. 6J″).

DISCUSSION

In this study, we conducted quantitative live-imaging of *A. coerulea* FMs to investigate the growth dynamics of floral organ initiation, and FM proliferation and termination. Growth is defined as an increase in cell volume and area, which can be driven by cell expansion alone, or the combination between cell expansion and cell division (Steeves and Sussex, 1989). We paid attention to both phenomena because many previous studies have suggested that these processes could be governed by distinct molecular programs and hormonal pathways (Ioio et al., 2008; Perrot-Rechenmann, 2010; Besnard et al., 2014; Chandler and Werr, 2015; Mambro et al., 2017). As with any live-imaging study, this one comes with a series of caveats that are common to the field. For one, growth dynamics were measured in a strictly *in vitro* culturing system that cannot be quantitatively compared to *in vivo* growth rates. To address this concern, we examined multiple biological replicates for every growth window, which underwent very similar developmental processes and showed consistent morphological landmarks from previous ontogenetic studies (Tucker and Hodges, 2005). In addition, similar to most live-imaging studies, our analysis was limited to surface reconstruction of the cells, although it is well known that many developmental processes in primordium initiation and meristem proliferation are driven by cellular changes underneath the epidermal surfaces (e.g. Hill and Lord, 1989). Even given these caveats, there is much that can be learned from these studies regarding developmental processes that may be broadly conserved across flowering plant lineages.

Cellular dynamic change during FMT in *A. coerulea*

Over the past few decades, studies using mitotic index and clonal sectors have revealed that most meristems are highly organized structures, composed of a central zone (CZ) and a peripheral zone (PZ), which harbor the stem cells and organogenic cells, respectively (Stewart and Dermen, 1970; Marc and Palmer, 1982; Steeves and Sussex, 1989). Thus, the maintenance of stem cell identity in the CZ is key to meristem indeterminacy. Many key genes controlling meristem homeostasis have been identified, and perhaps the most crucial is the stem cell identity gene *WUSCHEL* (*WUS*), which is exclusively expressed at the base of the CZ (Laux et al., 1996; Mayer et al., 1998). Therefore, when we consider the FMT process, we are explicitly asking when and how *WUS* expression is permanently downregulated.

Despite its essential role in floral development, little is known about meristem dynamics during FMT at a cellular level, and the molecular basis of FMT has only been investigated in *A. thaliana* and tomato (Sun et al., 2009; 2014; Bollier et al., 2018). In *A. thaliana*, the downregulation of *WUS* coincides with the initiation of carpel primordia, and the precise timing of *WUS* repression is considered a key factor that determines the number of cells produced for carpel development (Sun et al., 2009; 2014; Sun and Ito, 2015). However, it remains to be seen whether these genetic mechanisms are more broadly conserved and, perhaps most importantly, whether both of these models have rather simple flowers with only four whorls of organs, representing only a small fraction of the diversity seen in angiosperms (Endress, 1990).

Previous transcriptomic sequencing in young *A. coerulea* FMs indicated that the expression of *AqWUS* is maintained during the developmental stages equivalent to TP1 through TP3 in the current study, with expression dropping rapidly to undetectable levels during the developmental stages equivalent to TP4 to TP6 (Min and Kramer, 2020). If we examine the central region of the FM (i.e. bin1 and bin2 in the growth alignment graphs, Fig. 3F), which roughly corresponds to the central zone, we did observe similarly low numbers of cell divisions between TP1 and TP3 (Fig. 3F; Table S1), with bin2 being higher than bin1. During TP4 to TP6, which corresponds to the early stages of carpel development, the average number of cell divisions in the center of the floral apex was close to zero (Fig. 3F; Table S1). However, most strikingly, we observed a higher number of cell divisions in the center of the floral apex between TP3 and TP4, during which the carpel primordia are initiated (Fig. 3C,C′,F), with the bin1 values being statistically significantly higher than all other stages (Fig. 3F; Table S1).

This observation raises some intriguing questions: why is there an increase in cell division in the central zone when the carpel primordia are initiating, and what is responsible for the pattern? This period also appears to correspond with the onset of FMT based on the decline in *AqWUS* expression (Min and Kramer, 2020), so is this the last flush of CZ cell divisions or are the divisions related more directly to initiation of the carpel primordia? Answering these questions will require a better understanding of how *AqWUS* downregulation is controlled in *Aquilegia*, particularly the nature of any ‘timer mechanism’ regulating the number of cell divisions before FMT. In the FMs of *A. thaliana* and tomato, the gene *KNUCKLES* (*KNU*) is activated in a cell division-dependent manner, which determines the temporal control of FMT, as, once *KNU* is activated, it terminates the expression of *WUS*. Manipulation of cell cycles in the FM can accelerate or delay the activation of *KNU*, which results in the premature or delayed termination of the FM, respectively (Sun et al., 2014). We currently do not know whether the *KNU*-*WUS* pathway is conserved in other angiosperm systems, especially taxa with more than one whorl of stamens and unfused carpels but, even if it is not conserved, it will be interesting to examine whether a division-dependent timing mechanism is used for FMT in general. Overall, the combined patterns of cell behavior we observe at the center of the meristem during TP3-TP4 then transitioning into TP4-TP5, which include a sudden rise in divisions during TP3-TP4 and a sharp decline in cell expansion following this phase, appear to be markers for a loss of stem cell identity in this zone in conjunction with the FMT.

Development (2022) 149, dev200256. doi:10.1242/dev.200256

Floral organ primordia initiation in *A. coerulea*

In following the initiation of stamen, staminode and carpel primordia, we observed interesting dynamics in the relative growth behavior of the adaxial and abaxial cells (Figs. 4 and 5). First, only some of the cells that initially exhibited positive curvature in the NEP end up as adaxial cells in the primordium proper, with the adaxial-most cells being incorporated into the primordium boundary. Second, cells with negative surface curvature that were mainly located in the boundary region below the initial bulge ultimately become the cells exhibiting the highest growth rates. These high growth rates were primarily driven by highly anisotropic cell expansion that, coupled with later cell division, quickly promotes outgrowth of the abaxial surface of the primordium. This pattern is consistent with a previous study of expression of the abaxial polarity gene *AqFIL*, which is detected broadly across the entire ICP and most of the NEP (Fig. 1F), similar to the expression patterns of *FIL* in *A. thaliana* FMs (Meaders et al., 2020; Zhao and Traas, 2021). It is curious that cells exhibiting the highest growth rates are along the extreme abaxial margin of the primordium, representing only part of the typical abaxial domain, a pattern that has also been observed during leaf and sepal primordium initiation in *A. thaliana* (Zhao and Traas, 2021). A close examination of the spatial-temporal expression patterns of other polarity genes in *A. coerulea* will be a good starting point to decipher any potential difference in the abaxial cells, as well as the transition of cells that were originally in the adaxial surface but ended up in the organ boundary region.

The observed difference in the growth dynamics between sd1 and sd2 was more surprising. Once the primordia initiate as NEP, the growth rates of sd1 appeared to be lower than other NEP and ICP in other developmental intervals (Fig. 5L). Although the sd1 and sd2 whorls have the same staminode identity (Kramer et al., 2007; Sharma and Kramer, 2013), a previous study has observed subtle morphological differences that are apparent when the primordia are as small as 1-2 mm in length, most notably lateral marginal curling that facilitates late-stage adhesion between the organs (Meaders et al., 2020). In that study, the authors raised the issue of whether these differences were developmentally determined from the earliest stages or were due to some kind inductive interaction of the tissues. Our observation of differences from inception could suggest that they do harbor distinct developmental trajectories from their earliest stages, possibly implicating identity-based differences.

In addition, we examined the early developmental processes of the carpel primordia in detail, capturing a transition from growth that is mainly driven by strong anisotropic cell expansion to one that is promoted by concentrated cell divisions (Fig. 6). The initial cell expansion phase helps to lift the carpel primordia up, while the cell division phase appears to sculpt their shape (Fig. 5I,K; Fig. 6). The first phase of cell expansion seems to be very similar to the initiation of the stamen and staminodes, which was likewise driven by strong anisotropic expansion by a small number of abaxial cells (Fig. 5). However, the second phase of carpel growth is quite different than the other organs in that there is a much stronger reliance on accumulation of cell divisions while the cell areas did not expand significantly (e.g. st1 in Fig. 4 compared with Fig. 6). This observation could suggest that we observed a transition between two sets of molecular programs during early carpel primordia growth: one for the earliest phase of primordia initiation that is common to all floral organs and the subsequent program that is specific to sculpting carpel primordia.

Conclusions

FM development is crucial to the reproductive success of a plant and is distinct from shoot meristem development for many reasons, including the fact that these meristems are determinate and undergo FMT. In-depth investigation of meristem behavior requires not only knowledge of different molecular regulatory networks, but also how such networks directly control precise patterns cell division and expansion over time. Overall, the findings of this study shed new light on the dynamic processes that control floral primordia initiation and FMT. Our results have revealed how the dynamics between cell proliferation and expansion change as the FM transitions from production of stamens to staminodes to carpels, and uncovered distinct patterns of primordium initiation between stamens and staminodes compared with carpels, as well as subtle distinctions between the two whorls of staminodes. With regard to FMT, this is the first live-imaging study of this process in any plant system, and it remains to be seen how similar the syncarpous development of other major models compares with the apocarpous pattern expressed here. We are particularly intrigued by the observation that the process of FMT is discernable based on cell division dynamics preceding carpel initiation and expect that combining our live-imaging technique with future gene expression approaches will help resolve the significance of these patterns.

MATERIALS AND METHODS

Plant materials, growth conditions and dissection

Seeds of *Aquilegia×coerulea* ‘Kiragami’ were purchased from Swallowtail Garden Seeds (Santa Rosa, CA, USA) and germinated in damp soil. The regular growth condition for seedlings and young plants is 16 h daylight at 18°C and 8 h dark at 13°C, with humidity under 40%. Once the plants developed approximately six true leaves, they were transferred into vernalization conditions (16 h daylight at 6°C and 8 h dark at 6°C) for 3-4 weeks, and then moved back to the regular growth conditions. When the primary inflorescences started to develop, young side branches with axillary meristems were cut off from the plant, washed in 10% bleach for 20 min and then thoroughly rinsed with double-distilled water three times. Axillary meristems on the branches were then dissected using a surgical needle under a dissecting microscope. After all the sepals were removed, the floral meristems placed on a petri dish with tissue culture medium composed of 0.5× Linsmaier & Skoog medium (Caisson Labs), with 3% sucrose, 0.8% UltraPure Agarose (Invitrogen), 10^{-6} M kinetin (MilliporeSigma) and 10^{-7} M gibberellic acid (GA3, MilliporeSigma). The Petri dishes were placed in a tissue culture growth chamber with 16 h light at 20°C and 8 h dark at 13°C.

Imaging

FMs were stained with 0.5 mg/ml propidium iodide solution in double-distilled water (Sigma-Aldrich) by immersing the tissue in stain solution for 2.5 min for the initial timepoint and then for 2 min for subsequent timepoints. The stain was removed, and the tissue washed in double-distilled water three times. Meristems were imaged immediately after staining using a LSM 980 NLO Multi-photon confocal laser scanning microscope (Zeiss) equipped with a water immersion objective (W Plan-Apochromat 20×/1.0 DIC UV-IR M27 75 mm). A DPSS 514 nm laser was used for excitation, and emissions were collected between 580-670 nm. Scans were frame averaged twice and *z*-sections taken at 2 µm intervals. After imaging, the remaining water in the petri dishes was carefully removed using a pipette and the petri dishes were returned to the issue culture growth chamber. All samples were imaged every 48 h, and most of the samples were imaged up to three or four times (i.e. 3-4 TPs). Because, in the current study, we have sampled a developmental window spanning six TPs in total, we have stacked multiple independent time-lapse imaging series to cover the six TPs. For example, there are four independent time-lapse images that span equivalent stages to TP1-TP4, and four independent time-lapse images that span equivalent stages to TP3-TP6. Every successive TP interval had at least three biological replicates (i.e. independent time-lapse imaging sessions), which were also used as biological replicates to construct the growth alignment graphs (Fig. 3F). Stacking several time-lapse experiments (with replicates) to achieve a larger developmental

window is common in long-term live-imaging studies (e.g. Kuchen et al., 2012; Kierzkowski et al., 2019).

Imaging processing and data analysis

The confocal image files were transformed into .tif files in ImageJ (https://imagej.nih.gov/ij/) and processed in MorphoGraphX (https://morphographx.org/). Briefly, all image stacks were Gaussian Blurred twice with a radius of 1 on all X/Y/Z sigma, and all meshes were subdivided and smoothed (with 10 passes for each smooth) three times. Cells on the surfaces were segmented using auto-segmentation, and all the segmentation errors were corrected manually. Heat-map graphs and values were generated using MorphoGraphX, and statistical analysis (ANOVA, Tukey's HSD) was carried out in R (version 1.1.456). For the growth alignment graphs, we had four biological replicates for every developmental interval, except TP5-TP6, which had three biological replicates. The distance between the center of each floral apex to the edge of the newly emerged primordia (NEP; defined in the Results) was normalized and divided into six equal bins. For each bin, the biological replicates were pooled and means for cell area expansion and cell division were calculated.

Acknowledgements

The authors thank Mingyuan Zhu, Daniel Kierzkowski, Anne-Lise Routier-Kierzkowska, Richard Smith and Soeren Strauss for patiently answering all the questions about MorphoGraphX, and Weilin Meng for generously lending his PC during the entire Covid-19 pandemic, on which we conducted all the image processing and analysis.

Competing interests

The authors declare no competing or financial interests.

Author contributions

Conceptualization: Y.M., E.M.K.; Methodology: Y.M., S.J.C.; Software: Y.M., S.J.C.; Validation: Y.M., S.J.C.; Formal analysis: Y.M., S.J.C., E.M.K.; Investigation: Y.M., S.J.C., E.M.K.; Data curation: Y.M., S.J.C.; Writing - original draft: Y.M.; Writing - review & editing: Y.M., S.J.C., E.M.K.; Visualization: Y.M., S.J.C.; Supervision: E.M.K.; Project administration: E.M.K.; Funding acquisition: Y.M., E.M.K.

Funding

This study was funded by an Emerging Models Award to Y.M. from the Society of Developmental Biology.

Peer review history

The peer review history is available online at https://journals.biologists.com/dev/article-lookup/doi/10.1242/dev.200256.

References

Barbier de Reuille, P., Routier-Kierzkowska, A.-L., Kierzkowski, D., Bassel, G. W., Schüpbach, T., Tauriello, G., Bajpai, N., Strauss, S., Weber, A., Kiss, A. et al. (2015). MorphoGraphX: A platform for quantifying morphogenesis in 4D. *eLife* **4**, e05864.

Bartlett, M. E. and Thompson, B. (2014). Meristem identity and phyllotaxis in inflorescence development. *Frontiers in Plant Science* **5**, 508. doi:10.3389/fpls.2014.00508

Besnard, F., Rozier, F. and Vernoux, T. (2014). The AHP6 cytokinin signaling inhibitor mediates an auxin-cytokinin crosstalk that regulates the timing of organ initiation at the shoot apical meristem. *Plant Signaling & Behavior* **9**, e28788. doi:10.4161/psb.28788

Bollier, N., Sicard, A., Leblond, J., Latrasse, D., Gonzalez, N., Gévaudant, F., Benhamed, M., Raynaud, C., Lenhard, M., Chevalier, C. et al. (2018). At-MINI ZINC FINGER2 and SI-INHIBITOR OF MERISTEM ACTIVITY, a conserved missing link in the regulation of floral meristem termination in arabidopsis and tomato. *Plant Cell* **30**, 83-100. doi:10.1105/tpc.17.00653

Chandler, J. W. and Werr, W. (2015). Cytokinin–auxin crosstalk in cell type specification. *Trends Plant Sci.* **20**, 291-300. doi:10.1016/j.tplants.2015.02.003

Endress, P. K. (1990). Patterns of floral construction in ontogeny and phylogeny. *Biol. J. Linn. Soc.* **39**, 153-175. doi:10.1111/j.1095-8312.1990.tb00509.x

Filiault, D. L., Ballerini, E. S., Mandáková, T., Aköz, G., Derieg, N. J., Schmutz, J., Jenkins, J., Grimwood, J., Shu, S., Hayes, R. D. et al. (2018). The Aquilegia genome provides insight into adaptive radiation and reveals an extraordinarily polymorphic chromosome with a unique history. *eLife* **7**, e36426. doi:10.7554/eLife.36426

Hamant, O., Das, P. and Burian, A. (2019). Time-lapse imaging of developing shoot meristems using a confocal laser scanning microscope. *Methods in Molecular Biology (Clifton, N.J.)* **1992**, 257-268. doi:10.1007/978-1-4939-9469-4_17

Harrison, C. J., Roeder, A. HK., Meyerowitz, E. M. and Langdale, J. A. (2009). Local cues and asymmetric cell divisions underpin body plan transitions in the moss physcomitrella patens. *Curr. Biol.* **19**, 461-471. doi:10.1016/j.cub.2009.02.050

Heisler, M. G. and Ohno, C. (2014). Live-Imaging of the Arabidopsis Inflorescence Meristem. In *Methods in Molecular Biology. Flower Development* (ed. J. L. Riechmann and F. Wellmer), pp. 431-440. New York, NY: Springer New York.

Hill, J. P. and Lord, E. M. (1989). Floral development in *Arabidopsis thaliana*: a comparison of the wild type and the homeotic pistillata mutant. *Can. J. Bot.* **67**, 2922-2936. doi:10.1139/b89-375

Ioio, R. D., Nakamura, K., Moubayidin, L., Perilli, S., Taniguchi, M., Morita, M. T., Aoyama, T., Costantino, P. and Sabatini, S. (2008). A genetic framework for the control of cell division and differentiation in the root meristem. *Science* **322**, 1380-1384. doi:10.1126/science.1164147

Kierzkowski, D., Runions, A., Vuolo, F., Strauss, S., Lymbouridou, R., Routier-Kierzkowska, A.-L., Wilson-Sánchez, D., Jenke, H., Galinha, C., Mosca, G. et al. (2019). A growth-based framework for leaf shape development and diversity. *Cell* **177**, 1405-1418.e17. doi:10.1016/j.cell.2019.05.011

Kirchoff, B. K. and Claßen-Bockhoff, R. (2013). Inflorescences: concepts, function, development and evolution. *Annals of Botany* **112**, 1471-1476. doi:10.1093/aob/mct267

Kramer, E. M. (2009). *Aquilegia*: a new model for plant development, ecology, and evolution. *Annu. Rev. Plant Biol.* **60**, 261-277.

Kramer, E. M., Holappa, L., Gould, B., Jaramillo, M. A., Setnikov, D. and Santiago, P. M. (2007). Elaboration of B gene function to include the identity of novel floral organs in the lower eudicot *Aquilegia*. *Plant Cell* **19**, 750-766. doi:10.1105/tpc.107.050385

Kuchen, E. E., Fox, S., Reuille, P. B. de, Kennaway, R., Bensmihen, S., Avondo, J., Calder, G. M., Southam, P., Robinson, S., et al. (2012). Generation of leaf shape through early patterns of growth and tissue polarity. *Science* **335**, 1092-1096. doi:10.1126/science.1214678

Laux, T., Mayer, K. F., Berger, J. and Jürgens, G. (1996). The WUSCHEL gene is required for shoot and floral meristem integrity in Arabidopsis. *Development (Cambridge, England)* **122**, 87-96. doi:10.1242/dev.122.1.87

Mambro, R. D., Ruvo, M. D., Pacifici, E., Salvi, E., Sozzani, R., Benfey, P. N., Busch, W., Novak, O., Ljung, K., Paola, L. D. et al. (2017). Auxin minimum triggers the developmental switch from cell division to cell differentiation in the Arabidopsis root. *Proc. Natl Acad. Sci. USA* **114**, E7641-E7649.

Marc, J. and Palmer, J. H. (1982). Changes in mitotic activity and cell size in the apical meristem of Helianthus Annuus L. During the transition to flowering. *Am. J. Bot.* **69**, 768-775.

Mayer, K. FX., Schoof, H., Haecker, A., Lenhard, M., Jürgens, G. and Laux, T. (1998). Role of WUSCHEL in regulating stem cell fate in the arabidopsis shoot meristem. *Cell* **95**, 805-815. doi:10.1016/S0092-8674(00)81703-1

Meaders, C., Min, Y., Freedberg, K. J. and Kramer, E. (2020). Developmental and molecular characterization of novel staminodes in Aquilegia. *Annals of Botany* **126**, 231-243. doi:10.1093/aob/mcaa029

Min, Y. and Kramer, E. M. (2020). Transcriptome profiling and weighted gene co-expression network analysis of early floral development in Aquilegia coerulea. *Sci. Rep.* **10**, 19637. doi:10.1038/s41598-020-76750-7

Monniaux, M., Pieper, B., McKim, S. M., Routier-Kierzkowska, A.-L., Kierzkowski, D., Smith, R. S. and Hay, A. (2018). The role of APETALA1 in petal number robustness. *eLife* **7**, e39399. doi:10.7554/eLife.39399

O'Connor, D. L. (2018). Live confocal imaging of Brachypodium Spikelet meristems. *Bio-protocol* **8**, e3026-e3026.

Perrot-Rechenmann, C. (2010). Cellular responses to Auxin: division versus expansion. *Cold Spring Harbor Perspect. Biol.* **2**, a001446.

Prunet, N. and Duncan, K. (2020). Imaging flowers: a guide to current microscopy and tomography techniques to study flower development (F Wellmer, Ed.). *J. Exp. Bot.* **71**, 2898-2909. doi:10.1093/jxb/eraa094

Prunet, N., Jack, T. P. and Meyerowitz, E. M. (2016). Live confocal imaging of Arabidopsis flower buds. *Dev. Biol.* **419**, 114-120. doi:10.1016/j.ydbio.2016.03.018

Prunet, N., Yang, W., Das, P., Meyerowitz, E. M. and Jack, T. P. (2017). *SUPERMAN* prevents class B gene expression and promotes stem cell termination in the fourth whorl of *Arabidopsis thaliana* flowers. *Proc. Natl Acad. Sci. USA* **114**, 7166-7171.

Rahni, R. and Birnbaum, K. D. (2019). Week-long imaging of cell divisions in the Arabidopsis root meristem. *Plant Methods* **15**, 30. doi:10.1186/s13007-019-0417-9

Reddy, G. V. and Roy-Chowdhury, A. (2009). Live-imaging and image processing of shoot apical meristems of Arabidopsis thaliana. *Methods in Molecular Biology (Clifton, N.J.)* **553**, 305-316. doi:10.1007/978-1-60327-563-7_15

Refahi, Y., Zardilis, A., Michelin, G., Wightman, R., Leggio, B., Legrand, J., Faure, E., Vachez, L., Armezzani, A., Risson, A.-E. et al. (2021). A multiscale analysis of early flower development in Arabidopsis provides an integrated view of molecular regulation and growth control. *Dev. Cell* **56**, 540-556.e8. doi:10.1016/j.devcel.2021.01.019

Roeder, A. HK., Chickarmane, V., Cunha, A., Obara, B., Manjunath, B. S. and Meyerowitz, E. M. (2010). Variability in the control of cell division underlies sepal epidermal patterning in Arabidopsis thaliana. *PLoS Biol.* **8**, e1000367. doi:10.1371/journal.pbio.1000367

Sappl, P. G. and Heisler, M. G. (2013). Live-imaging of plant development: latest approaches. *Curr. Opin. Plant Biol.* **16**, 33-40. doi:10.1016/j.pbi.2012.10.006

Sharma, B. and Kramer, E. (2013). Sub- and neo-functionalization of *APETALA3* paralogs have contributed to the evolution of novel floral organ identity in *Aquilegia* (columbine, Ranunculaceae). *New Phytol.* **197**, 949-957. doi:10.1111/nph.12078

Steeves, T. A. and Sussex, I. M. (1989). *Patterns in Plant Development*. Cambridge University Press.

Stewart, R. N. and Dermen, H. (1970). Determination of number and mitotic activity of shoot apical initial cells by analysis of mericlinal chimeras. *Am. J. Bot.* **57**, 816-826. doi:10.1002/j.1537-2197.1970.tb09877.x

Sun, B. and Ito, T. (2015). Regulation of floral stem cell termination in Arabidopsis. *Frontiers Plant Sci.* **6**, 17. doi:10.3389/fpls.2015.00017

Sun, B., Xu, Y., Ng, K.-H. and Ito, T. (2009). A timing mechanism for stem cell maintenance and differentiation in the Arabidopsis floral meristem. *Genes Dev.* **23**, 1791-1804. doi:10.1101/gad.1800409

Sun, B., Looi, L.-S., Guo, S., He, Z., Gan, E.-S., Huang, J., Xu, Y., Wee, W.-Y. and Ito, T. (2014). Timing mechanism dependent on cell division is invoked by polycomb eviction in plant stem cells. *Science* **343**, 1248559-1248559. doi:10.1126/science.1248559

Tucker, S. C. and Hodges, S. A. (2005). Floral ontogeny of *Aquilegia*, *Semiaquilegia*, and *Enemion* (Ranunculaceae). *Int. J. Plant Sci.* **166**, 557-574. doi:10.1086/429848

Zhang, T., Cieslak, M., Owens, A., Wang, F., Broholm, S. K., Teeri, T. H., Elomaa, P. and Prusinkiewicz, P. (2021). Phyllotactic patterning of gerbera flower heads. *Proc. Natl Acad. Sci. USA* **118**, e2016304118.

Zhao, F. and Traas, J. (2021). Stable establishment of organ polarity several plastochrons before primordium outgrowth in Arabidopsis. *Development* **148**, dev.198820. doi:10.1242/dev.198820